ARMA 15-0855

APPLICATIONS OF HYDRO-MECHANICALLY COUPLED 3D MINE AND RESERVOIRE SCALE, DISCONTINUOUS, STRAIN-SOFTENING DILATANT MODELS WITH DAMAGE

Flatten, A.
Beck Engineering Pty Ltd, Berlin, Germany
Beck, D.
Beck Engineering Pty Ltd, Sydney, NSW, Australia

This paper was prepared for presentation at the 49th US Rock Mechanics / Geomechanics Symposium held in San Francisco, CA, USA, 28 June-1 July 2015.

ABSTRACT: In gas and oil as well as in several mining applications hydro-mechanical phenomena play an important role and need to be considered in numerical models for calibration and forecasting analyses. In this paper, a two-way coupled hydro-mechanical formulation is described and applied to real size, complex 3D mining and reservoir model examples including structures using the Finite-Element Method (FEM) framework. The proposed coupling considers increasing hydraulic conductivities due to the evolution of rock mass damage induced by mining activities or fluid injection. This enables the potential development of additional flow paths and affects the fluid pressure distribution, which, in turn, affects the mechanical response via the effective stress concept. The mechanical framework uses a strain-softening, dilatant and discontinuum constitutive model for both bulk rockmass and structures such as faults on a regional scale and discrete fracture networks (DFN).

1. INTRODUCTION

Hydro-mechanical phenomena for geotechnical extraction applications, as in the mining or gas and oil industries, are very important aspects of global or well stability, subsidence and in some cases, accurate forecasting of recovery. Most adverse rock related hydro-mechanical phenomena are stress path dependent. Uncoupled or loosely coupled modelling of flow or rock deformation is therefore not ideal; the important fluid rock coupling is over-simplified, or else, the stress path may not be replicated with high similitude.

Here, we present closely and fully coupled, parallel solution formulation adopting single and multi-phase, multi-component fluid flow formulations into a discontinuum, strain softening, and dilatant Finite Element model. Particular emphasis is on the nonlinear coupling of the deformable and strain softening solid skeleton and the fluid phase(s), e.g. the change of hydraulic properties with evolution of damage in the matrix material as well as the effect of pore pressures on the overall stress distribution. This governing system of coupled nonlinear partial differential equations is embedded in the framework of a Finite-Element (FE) algorithm and applied to various large-scale real-life mine and reservoir models.

The main benefit for practical reservoir engineering is that rock mechanics processes including damage, seismicity and deformation are likely to be better replicated with the fully coupled model than with partly coupled or uncoupled models. This should enable more direct calibration and potentially a closer replication of field observations for higher model reliability.

In section 2 both the mechanical and hydrological formulations are described independently. In section 3, the coupling quantities are emphasized, and the different coupling approaches are discussed. Three numerical examples are presented; (i) an underground coal mining simulation, (ii) open pit excavation simulation and (iii) reservoir depletion simulation are investigated in section 4. The paper closes with a summary in section 5.

2. BASIC MODEL FORMULATIONS

2.1. Mechanical formulation

The main focus is on the constitutive relations; however for the sake of completeness we also briefly state the governing balance equation and kinematics first.

The quasi-static linear and angular momentum

$$\mathrm{div}(\boldsymbol{\sigma}) = \rho \boldsymbol{b}_f, \qquad \boldsymbol{\sigma}^T = \boldsymbol{\sigma} \tag{1}$$

are given in terms of (total) Cauchy stresses $\boldsymbol{\sigma}$, bulk mass density ρ and volumetric forces $\boldsymbol{b}_f$. Eq.(1) is defined in the deformed domain configuration.

As strain rate measure, the rate-of-deformation

$$\boldsymbol{D} = \nabla^{sym}(\boldsymbol{v}), \qquad \boldsymbol{D} = \boldsymbol{D}_E + \boldsymbol{D}_P \tag{2}$$

is introduced, which can be additively decomposed in an elastic and plastic part. Here, $\boldsymbol{v}$ denotes the velocity field, $\boldsymbol{v} = d\boldsymbol{u} \,/\, dt$, with $\boldsymbol{u}$ being the displacement field. The Cauchy stresses can be updated from a material objective stress rate $\boldsymbol{\sigma}^{\circ}$, which is obtained as action of the elasticity tensor $\boldsymbol{\mathcal{C}}_E$ on the elastic part of the rate-of-deformation

$$\boldsymbol{\sigma}^{\circ} = \boldsymbol{\mathcal{C}}_E \cdot (\boldsymbol{D} - \boldsymbol{D}_P). \tag{3}$$

It remains to quantify the plastic part of the rate-of-deformation, which is presented in the reminder of this subsection.

The Menetry-Williams [1] yield surface

$$f(p,q,r) = \left(\frac{q}{\sigma_{ci}}\right)^2 + m_b \left(\frac{1}{3}\frac{q}{\sigma_{ci}} R(r/q\,,e) - \frac{p}{\sigma_{ci}}\right) - s \tag{4}$$

is defined as function of the three stress invariants

$$p = -\frac{1}{3}\mathrm{tr}(\boldsymbol{\sigma}), \qquad \text{hydrostatic pressure} \tag{5}$$

$$q = \left(\frac{3}{2}\boldsymbol{\sigma}' \cdot \boldsymbol{\sigma}'\right)^{\frac{1}{2}}, \qquad \text{Mises equiv. stress} \tag{6}$$

$$r = \left(\frac{9}{2}\boldsymbol{\sigma}' \cdot (\boldsymbol{\sigma}'\boldsymbol{\sigma}')\right)^{1/3}, \qquad \text{3rd stress invariant} \tag{7}$$

with $\boldsymbol{\sigma}'$ being the deviatoric part of the Cauchy stresses, $\boldsymbol{\sigma}' = \mathrm{dev}(\boldsymbol{\sigma})$.

The material parameters in this formulation are given by σ_{ci}, s, m_b and e, where σ_{ci} represents the uniaxial compressive strength and s and m_b are measures of the cohesive and frictional strengths. Further, e represents the deviatoric eccentricity, that describes the out-of-roundness of the yield surface in the deviatoric plane.

Using the deviatoric polar angle θ as substitution, defined as

$$\cos 3\theta = (r/q)^3, \tag{8}$$

the function $R(r/q, e)$ in eq.(4) can be expressed as

$$\breve{R}(\theta,e) = [4(1-e^2)\cos^2\theta + (2e-1)^2] \,/\, [\,2(1-e^2)\cos\theta + (2e-1)\sqrt{4(1-e^2)\cos^2\theta + 5e^2 - 4e}\,]. \tag{9}$$

Therefore, the eccentricity parameter is bound between $0.5 \le e \le 1.0$, where $e = 1$ results in a perfectly circular yield curve within the deviatoric plane, and $e = 0.5$ in a circumscribing approximation of the Hoek-Brown strength criterion [2].

The constitutive relations are completed by the non-associative flow rule

$$\boldsymbol{D}_P = \dot{\lambda}\frac{dG}{d\boldsymbol{\sigma}} \tag{10}$$

with plastic strain rate $\boldsymbol{D}_P$, equivalent plastic strain rate $\dot{\lambda}$ and the Levkovitch-Reusch (LR2, see [3]) plastic flow potential

$$G(p,q,r) = \left(\frac{q}{\sigma_{ci}}\right)^{1/a} + m_b \left(\frac{1}{3}\frac{q}{\sigma_{ci}} R(r/q,e) - d_g \frac{p}{\sigma_{ci}}\right) \tag{11}$$

In addition to those material parameters already defined in eq.(2), the parameters a and d_g are introduced. The latter is defining the bulk dilation. In general, parameters s, m_b and d_g can be functions of the accumulated equivalent plastic strain $\lambda \equiv \varepsilon_P$. In particular, these functional dependencies allow for strain-softening behaviour. Typically, piecewise linear functions are used that represent interpolations between (i) peak, (ii) transitional, and (iii) residual states.

Using a large and continuously growing database of calibrated material parameter sets, an approach has been suggested in [4] to relate most of the above mentioned parameters to only UCS and GSI parameters, as those are the most frequently available parameters characterized on site. This approach serves as a valuable initial parameter estimation, whereas individual adjustments are required during the calibration process, which is always the basis of any forecasting analyses.

2.2. Hydrological formulation

In this section, we limit ourselves to the description of a single-phase fluid flow formulation through a porous medium. Mass continuity yields

$$\frac{d(\rho_w \phi s)}{dt} + \mathrm{div}(\rho_w\, \boldsymbol{q}_w) = 0 \tag{12}$$

where ρ_w denotes the fluid density, ϕ the porosity and s the saturation. Further, the fluid flux is related according to Darcy

$$\boldsymbol{q}_w = -k_w\, \nabla H \tag{13}$$

via the hydraulic gradient

$$\nabla H = \frac{\nabla p_w}{\rho_w g} + \nabla z \tag{14}$$

to the fluid-pressure gradient ∇p_w. Here, k_w is the hydraulic conductivity through the porous bulk material

and g is the gravitational magnitude and ∇z the direction of gravitation, typically $\nabla z = [0 \quad 0 \quad 1]^T$.

The coefficient representing the hydraulic conductivity commonly depends on the saturation via a relative permeability function $k_r(s)$, see [5], and can be easily expanded to anisotropic behavior as well. For most geomechanical applications an orthotropic conductivity approach is utilized. E.g., for layered sedimentary domains the in plane-conductivity differs by an order-of-magnitude from the out-of-plane conductivity. In this paper, we focus on an additional dependency with is subject to more detailed description in section 3.

3. COUPLING

3.1. Coupling terms

Mechanical damage due to the evolution of plastic deformation causes fragmentation of the bulk rock mass, allowing for additional flow paths, or at least, lead to an increased hydraulic conductivity. Stages of rockmass fragmentation are indicated in Fig. 1.

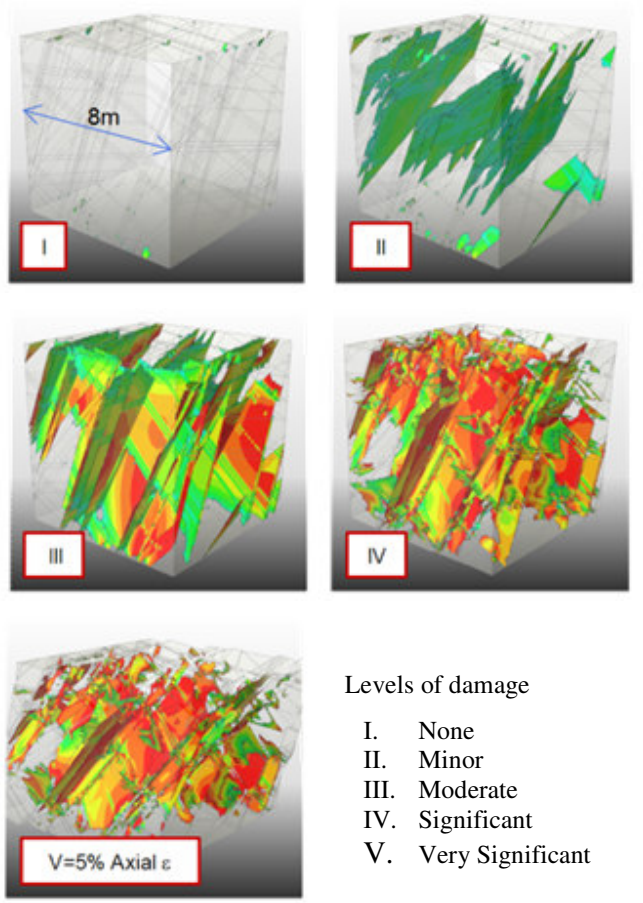

Fig. 1 Stages of plastic deformation, visualized using a modelled RVE with several arbitrary aligned and shaped discontinuum planes.

These considerations lead to a hydraulic conductivity function that depends on the rockmass damage, presented here as functional dependence of the equivalent plastic strain ε_P

$$k_w = f(\varepsilon_P). \tag{15}$$

In particular, the exponential relation

$$k_w(\varepsilon_P) = k_{w0} \exp\{A\varepsilon_P\} \leq k_{wmax} \tag{16}$$

is used within this paper, see Fig. 2, using a material dependent coefficient A and the initial (undamaged) conductivity k_{w0}. The increase is capped using a maximum conductivity k_{wmax}, which is typically in the order of 3-4 orders of magnitudes larger than the initial conductivity. However, alternative relations can be proposed and implemented easily.

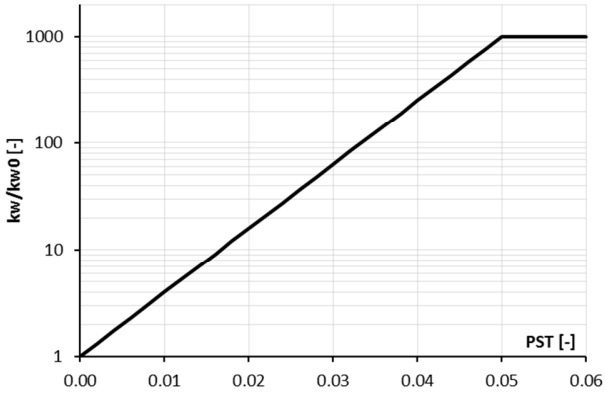

Fig. 2. Proposed relation, eq. (16), showing the increase in hydraulic conductivity with evolution of plastic strain on a logarithmic scale

On the other hand, in the other coupling direction, the effective stress concept of Terzaghi [6]

$$\boldsymbol{\sigma}^* = \boldsymbol{\sigma} + \alpha_B p_w \mathbf{1} \tag{17}$$

relates total stresses $\boldsymbol{\sigma}$ and effective stresses $\boldsymbol{\sigma}^*$ via the fluid pressure that is acting onto the solid skeleton of the porous medium $\alpha_B p_w$. Here, p_w is the wetting phase pressure in a general multi-phase flow analysis, or simply the pore-water pressure in single-phase groundwater analyses. The Biot coefficient α_B is generally bound between $0 < \alpha_B \leq 1$. Values for several different materials are given, for example in [7]. In eq. (17), the sign convention is such that stresses $\boldsymbol{\sigma}$ and $\boldsymbol{\sigma}^*$ are negative in compression, and p_w is positive in compression.

It is worth remembering that the total stresses $\boldsymbol{\sigma}$ are used to fulfill the balance equation, eq. (1). However, all constitutive relations are subject to the skeleton material and therefore eqs.(4)-(7),(10),(11) need to consider effective stresses $\boldsymbol{\sigma}^*$ in case of the presence of p_w.

3.2. *Coupling framework and terminology*

Each formulation is enriched with boundary conditions (prescribed displacement/fluid pressure or forces/flux at the respective model boundary) as well as initial conditions (initial stresses, porosity, etc over the whole model domain) and embedded in the Finite-Element (FE) concept.

Here, the mechanical formulation is implemented in an explicit FE framework, whereas the hydrological formulation is implemented in an implicit FE framework. The required information, i.e., plastic strain and fluid pressure, is exchanged at certain handshake times during the analysis before each analysis part can continue. In mining problems, at least the start of each new extraction step is required as handshake time, but the amount of handshakes within such an extraction step is generally not limited and should be increased until a converged solution is obtained.

We differentiate between three coupling 'directions':

- Uncoupled
- one-way coupled
- two-way coupled

as well as between three coupling 'densities':

- loosely coupled
- closely coupled
- fully coupled

Uncoupled analyses represent the classical mechanical-only (dry analysis) or hydrological-only (undamaged flow analysis) simulation runs. In one-way coupled analyses only the quantity of one simulation run is passed in the other run, but no information is returned, for example an entire flow analysis in performed using undamaged hydraulic conductivity properties, and the resulting fluid pressure is then included in the mechanical analysis via the effective stress concept. Depending on the problem being investigated those approaches are insufficient and two-way coupled analyses, as described in this paper, are required to closely match field observations.

The interval size between handshake time points at which information is exchanged between the two analysis runs determines the coupling density. The most economical way to exchange information is a loosely coupled scheme, which in turn may lead to an over-simplification of the hydro-mechanical phenomena. The smaller these time intervals become the better and more reliable the results get, at the disadvantage of increased computational cost. We characterize an analysis as a closely coupled scheme, if an increase in handshake points does not change the results noticeably. In addition, a fully coupled scheme allows for an exchange of data at each computational time increment in an explicit FE framework (technically, still being a staggered algorithm), or at each Newton iteration in an implicit FE framework.

4. EXAMPLES

4.1. *Underground coal mining*

This model comprises of several, mainly horizontally orientated sedimentary layers overlaying a coal seam of varying seam thicknesses between 10.-30.m at approximately 300.mRL. The top most overburden layers represent an aquifer, being separated from the coal seam by a layer representing an aquitard underneath.

The investigated mining method is a room-and-pillar approach over a footprint area of approx. 6.0 km².

Orthotropic hydraulic conductivities were required in order to replicate the intended fluid pressure profile within the upper overburden layers while draining the development within the coal seam underneath (Fig. 3).

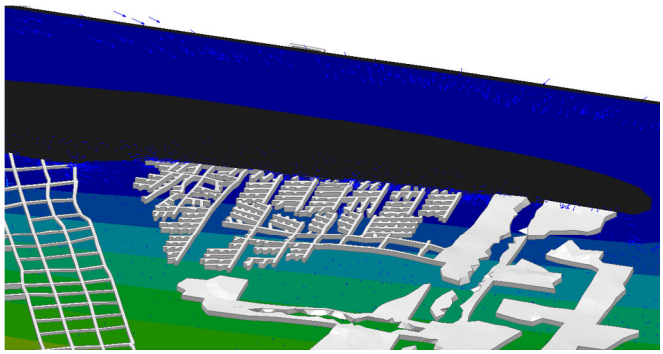

Fig. 3. Pore water pressure distribution on a vertical section showing the 3D mining excavations in the coal seam in grey. The dark zone above those mining excavations show the extend of drained material region.

As the mining excavations progress, damage in the coal pillars as well as in the overburden does evolve (Fig. 4), as well as occurrences of goafing can be examined. As a result, the modelled rockmass damage does not generally lead to a vertical hydraulic interconnectivity between upper aquifer and drained mining areas. However, within regions of weaker faults crossing the aquitard, damage within and around those faults evolves more quickly and more significantly, such that hydraulic interconnectivities form locally (Fig. 5).

As and additional outcome of the analysis, the subsidence is shown in Fig. 6.

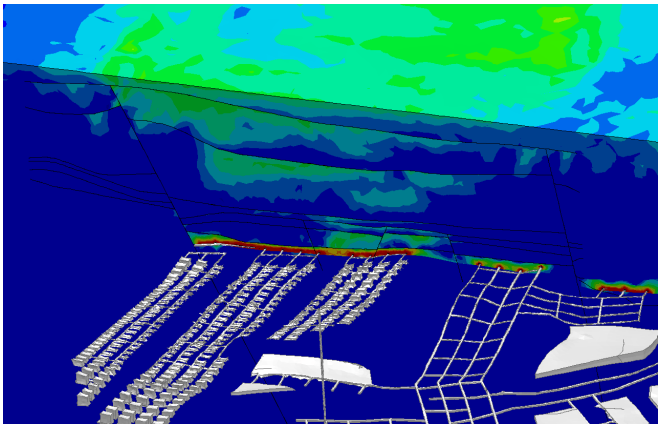

Fig. 4. Rockmass damage within the coal seam and overburden layers.

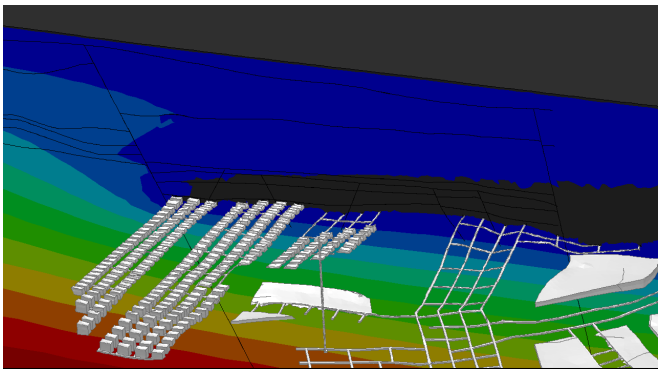

Fig. 5. Interconnection potential via damaged fault (right side of picture) crossing the aquitard (dark grey).

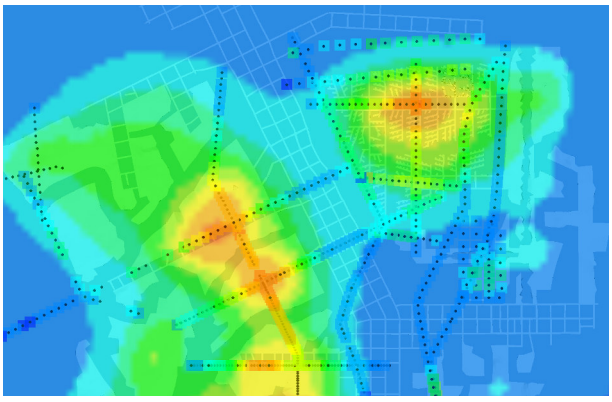

Fig. 6. Subsidence pattern.

4.2. *Open pit mining*

The presence of water in open pit projects adversely affects the slope stability. Depending on the pit geometry, geological setting as well as water recharge and drainage program, large pore water pressures can get relatively close to the free surface. In Fig. 7 and Fig. 8 typical distributions of pore water pressure and plastic strain are shown.

The effect of the fluid pressure onto the mechanical reponse is shown in Fig. 9. Here two cases are compared, (i) a dry case excluding effects of p_w, and (ii) a wet case including those effects. Note the substantially larger amount of damage for the wet case compared to dry case in regions near the pit surface and the pillar region (D).

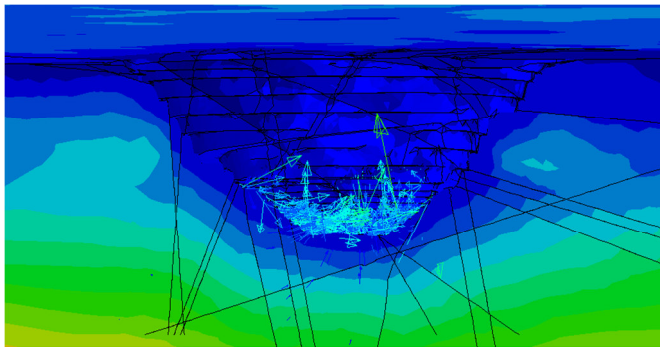

Fig. 7. Fluid pressure distribution surrounding the open pit excavation, including flux vectors at pit floor.

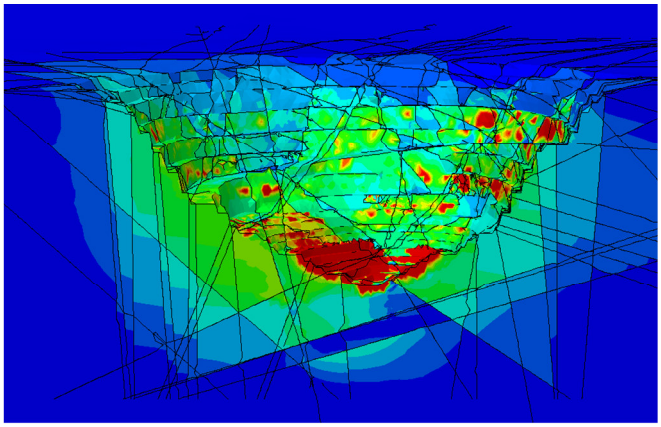

Fig. 8. Displacement pattern due to pit excavation and presence of pore water pressure.

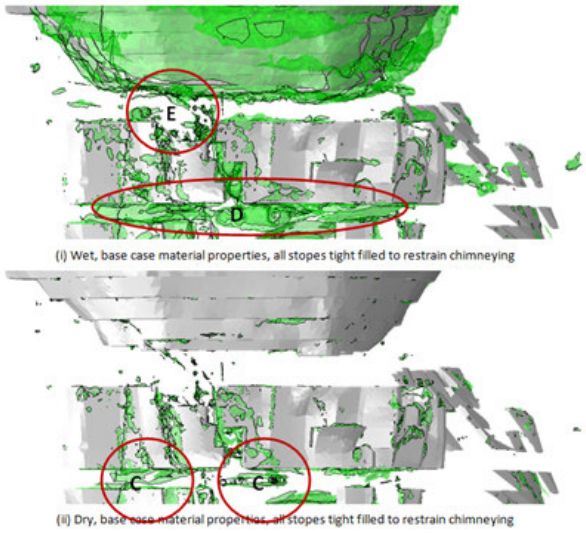

Fig. 9. Comparison of rockmass damage due to pit excavation with transition to underground stoping for cases (i) including and (ii) excluding effects of pore water pressure.

4.3. Reservoir depletion

This model comprises of two carbonate layers that are intersected by several fault structures. 17 wells are arranged to either produce fluid or inject water in the lower carabonate layer, see Fig. 10.

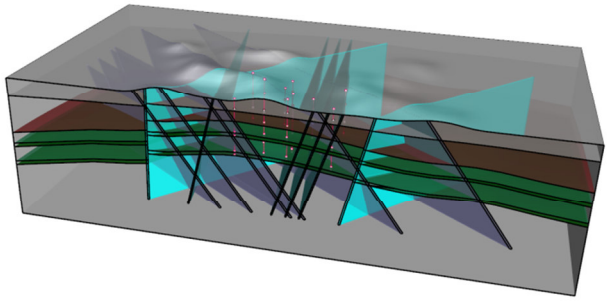

Fig. 10. Reservoir model, view cut showing different material domains and fault structures.

This model setup is used to study the differences between one-way and two-way coupling approaches, respectively. Whereas a one-way coupling analysis uses the effective stresses in the mechanical constitutive equations, only moderate damage evolves in regions surrounding an injection well. This rockmass damage is not coupled back to the fluid flow analysis, and as a consequence the hydraulic parameters are not updated, resulting in an unaffected fluid pressure distribution within each sequence step.

In contrast, for a two-way coupled approach, the rockmass damage in regions surrounding the injection wells does increase the hydraulic conductivity locally, which in turn affects the fluid pressure distribution. Due to these changes, again, even further damage might evolve, additionally changing the fluid pressure distribution, and so forth. For regions comprising only of a single homogenous material domain, this chain reaction will stop at some distance from the well, as fluid pressure changes do not contribute to significant damage evolution at that distance. However, in regions with spatially changing rock properties, this chain reaction may have different extents, as can be seen in regions where weaker faults are present in the near well surrounding. Such a case is shown in Fig. 11. Here, the resulting damage induced pressure distribution is such that the fault which is located at some distance from the well starts to yield. This yielding allows the fluid to enter the fault and to diffuse further into the structure. Any additionally injected water contributes to a further extend in this favourable direction, creating a new flow path across the fault.

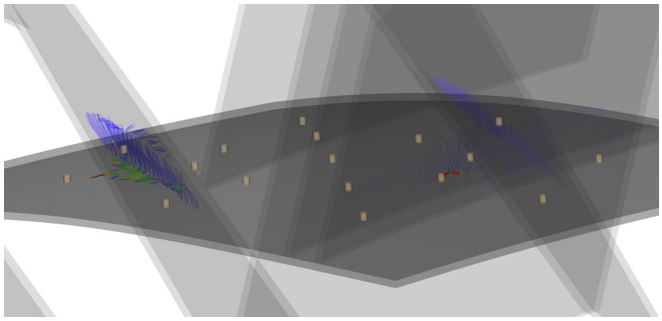

Fig. 11. Fluid flow along faults, which become additional, damage activated flow paths.

On the other hand, the increasing fluid pressure within the fault structure can destabilize the fault, yielding an increased fault slip potential. In the studied case, the dissipated plastic energy is used as a measure to quantify this potential, as shown in Fig. 12.

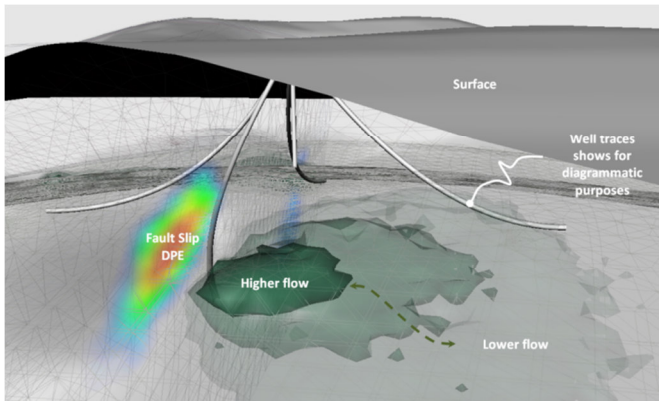

Fig. 12. Induced seismicity due to fluid pressure changes.

5. SUMMARY

The hydro-mechanically coupled model has been described in detail, with particular emphasis on the plastic strain evolution, as well as the damage-dependent hydraulic conductivity function. This framework is applied to real-sized, complex models including structures. The examples from mining and reservoir engineering applications show the importance of such a coupling framework in order to reproduce field observations with high similitude. Here, uncoupled or simplified one-way coupled results are compared with closely two-way coupled analysis results.

REFERENCES

[1] P. Menetrey und K. J. William, „Triaxial failure criterion for concrete and its generalization,“ *ACI Struct. J.,* Bd. 92, pp. 311-318, 1995.

[2] E. Hoek und E. T. Brown, „Empirical strength criterion for rock masses," *Journal of the Geotechnical Engineering Division,* Bd. 106, Nr. 9, pp. 1013-1035, 1980.

[3] V. Levkovitch, F. Reusch und D. A. Beck, „Application of a non-linear confinement sensitive constitutive model to mine scale simulations subject to varying levels of confining stress," in *Rock Mechanics in Civil and Environmental Engineering*, 2010.

[4] D. A. Beck, C. R. Lilley, F. Reusch, V. Levkovitch, G. Putzar und A. Flatten, „A preliminary, calibrated scheme for estimating rock mass properties for non-linear, discontinuum models," in *Sinorock*, 2013.

[5] M. T. van Genuchten, „A Closed-form Equation for Predicting the Hydraulic Conductivity of Unsaturated Soils," *Soil Sci. Am. J.,* Bd. 44, pp. 892-898, 1980.

[6] K. Terzaghi, „The shear resistance of saturated soils," in *International Conference on Soil Mechanics and Foundation Engineering*, Cambridge, MA, 1936.

[7] M. D. Zoback und J. D. Byerlee, „Permeability and effective stress," *AAPG Bull,* Bd. 59, pp. 154-158, 1975.